Article

Zn Protein Simulations Including Charge Transfer and Local Polarization Effects

Dmitri V. Sakharov, and Carmay Lim

J. Am. Chem. Soc., **2005**, 127 (13), 4921-4929• DOI: 10.1021/ja0429115 • Publication Date (Web): 12 March 2005

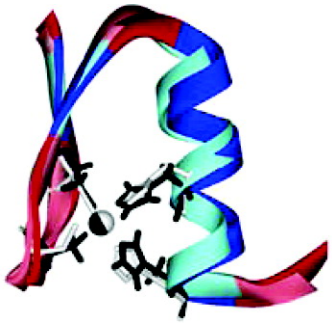

J|A|C|S
ARTICLES
Published on Web 03/12/2005

Zn Protein Simulations Including Charge Transfer and Local Polarization Effects

Dmitri V. Sakharov† and Carmay Lim*,†,‡

Contribution from the Institute of Biomedical Sciences, Academia Sinica, Taipei 115, and the Department of Chemistry, National Tsing Hua University, Hsinchu 300, Taiwan

Received November 24, 2004; E-mail: carmay@gate.sinica.edu.tw.

Abstract: Nearly half of all proteins contain metal ions, which perform a wide variety of specific functions associated with life processes. However, insights into the local/global, structural and dynamical fluctuations in metalloproteins from molecular dynamics simulations have been hampered by the "conventional" potential energy function (PEF) used in nonmetalloprotein simulations, which does not take into the nonnegligible charge transfer and polarization effects in many metal complexes. Here, we have carried out molecular dynamics simulations of Zn^{2+} bound to Cys^- and/or His^0 in proteins using both the conventional PEF and a novel PEF that accounts for the significant charge transfer and polarization effects in these Zn complexes. Simulations with the conventional PEF yield a nontetrahedral Cys_2His_2 Zn-binding site and significantly overestimate the experimental Zn−S(Cys^-) distance. In contrast, simulations with the new PEF accurately reproduce the experimentally observed tetrahedral structures of Cys_2His_2 and Cys_4 Zn-binding sites in proteins, even when the simulation started from a nontetrahedral Zn^{2+} configuration. This suggests that simulations with the new PEF could account for coordinational changes at Zn, which occurs during the folding/unfolding of Zn-finger proteins and certain enzymatic reactions The strategy introduced here can easily be applied to investigate Zn^{2+} interacting with protein ligands other than Cys^- and His^0. It can also be extended to study the interaction of other metals that have significant charge transfer and polarization effects.

Introduction

Zinc is an essential trace metal and is known to play important roles in biological systems.[1−14] It is a versatile ion as it can bind to different combinations of ligand types resulting in a broad range of stability, reactivity, and functions. Zn^{2+} can play either a predominantly catalytic role or a solely structural role to maintain the protein conformation. In particular, by coordinating to His^0 and/or Cys^- residues,[15] Zn^{2+} plays a critical role in the correct folding and stability of zinc-finger proteins, which are involved in various biological functions including DNA recognition, RNA packaging and dimerization, transcriptional activation, regulation of kinase activity and apoptosis, and lipid binding.[3,16]

An interesting property of Zn^{2+} that is important for its functional role in enzyme catalysis or protein folding/stability is its flexibility with respect to the number of first-shell ligands. In aqueous solution Zn^{2+} is octahedrally bound to six water molecules with an average Zn−O(water) distance of 2.10 Å.[17] In all zinc-finger proteins and most enzymes, Zn^{2+} is tetrahedrally coordinated, but in some catalytic sites, it is found to adopt a penta- or hexacoordinate geometry.[18] The coordination geometry has been found to depend on the type of ligand that is bound to Zn^{2+} and the solvent accessibility of the metal-binding site.[19] Furthermore, the decrease in the Zn^{2+} coordination number (CN) upon protein binding has been attributed mainly to (i) a solvent-inaccessible metal-binding site that enhances the electrostatic Zn−ligand interactions, (ii) the availability of vacant Zn^{2+} orbitals to accept charge from the ligands, and (iii) charge transfer from the amino acid ligands to the Zn cation, resulting in a lower positive charge on Zn; the weaker Zn−water electrostatic interactions and steric repulsion

† Academia Sinica.
‡ National Tsing Hua University.

(1) Vallee, B. L.; Auld, D. S. *Biochemistry* **1990**, *29*, 5647−5659.
(2) Christianson, D. W. *Adv. Protein Chem.* **1991**, *42*, 281−355.
(3) Coleman, J. E. *Annu. Rev. Biochem.* **1992**, *61*, 897−946.
(4) Lippard, S. J.; Berg, J. M. *Principles of Bioinorganic Chemistry*; University Science Books: Mill Valley, California, 1994.
(5) Schwabe, J. W. R.; Klug, A. *Nat. Struct. Biol.* **1994**, *1*, 345−349.
(6) Lipscomb, W. N.; Strater, N. *Chem. Rev.* **1996**, *96*, 2375−2433.
(7) Karlin, S.; Zhu, Z.-Y. *Proc. Natl. Acad. Sci. U.S.A.* **1997**, *94*, 14231−14236.
(8) Alberts, I. L.; Nadassy, K.; Wodak, S. J. *Protein Sci.* **1998**, *7*, 1700−1716.
(9) Lin, Y. L.; Lim, C. J. *J. Am. Chem. Soc.* **2004**, *126*, 2602−2612.
(10) Cox, E. H.; McLendon, G. L. *Curr. Opin. Chem. Biol.* **2000**, *4*, 162−165.
(11) McCall, K. A.; Huang, C.-C.; Fierke, C. A. *J. Nutr.* **2000**, *130*, 1437S−1446S.
(12) Laity, J. H.; Lee, B. M.; Wright, P. E. *Curr. Opin. Struct. Biol.* **2001**, *11*, 39−46.
(13) Dudev, T.; Lim, C. *J. Chin. Chem. Soc.* **2003**, *50*, 1093−1102.
(14) Dudev, T.; Lim, C. *Chem. Rev.* **2003**, *103*, 773−787.
(15) Gockel, P.; Vahrenkamp, H.; Zuberbuhler, A. D. *Helv. Chim. Acta* **1993**, *76*, 511−520.
(16) Berg, J. M.; Godwin, H. A. *Annu. Rev. Biophys. Biomol. Struct.* **1997**, *26*, 357.
(17) Marcus, Y. *Chem. Rev.* **1988**, *88*, 1475−1498.
(18) Dudev, T.; Lin, Y. L.; Dudev, M.; Lim, C. *J. Am. Chem. Soc.* **2003**, *125*, 3168−3180.
(19) Dudev, T.; Lim, C. *J. Am. Chem. Soc.* **2002**, *124*, 6759−6766.

among the ligand disfavor binding of water molecule(s) in the inner sphere, as compared to that in the outer sphere.[13,19]

Because of the significant charge transfer from protein ligands, especially Cys^-, to Zn^{2+} it is critical to include such effects in the potential energy function (PEF) describing the interactions of the Zn^{2+} ion with water molecules and protein atoms in computer simulations of Zn proteins. However, nearly all the current PEFs do not explicitly incorporate such charge-transfer effects, as the Zn^{2+} charge is constant (usually equal to +2e), irrespective of the number and type of ligands bound to Zn^{2+} during a simulation.[20] Furthermore, current PEFs generally do not explicitly include polarization effects, although a full +2e charge on Zn implicitly accounts for some of the polarization energy contributions. The current PEFs are generally based on either a (i) bonded, (ii) nonbonded, or (iii) semi-bonded model, as outlined below.

The *bonded* model of Zn−ligand interactions employs covalent bonds between Zn^{2+} and its ligands to maintain the Zn^{2+} coordination geometry in proteins during simulations.[21−25] For example, in simulations of carboxypeptidase A, explicit bond and angle terms were introduced between zinc, whose charge was reduced to 0.71e,[26] and the ligating atoms. Although *bonded* Zn−ligand interactions preserve the observed geometry of the metal-binding site, they would not be suitable in cases where (i) the metal-binding site is conformationally flexible, (ii) the CN of Zn^{2+} changes as in the folding/unfolding of Zn-finger proteins or in certain enzymatic reactions, and (iii) the Zn^{2+} ligands such as water molecules undergo exchange during the simulation.

The *nonbonded* model of Zn−ligand interactions relies on electrostatic and van der Waals (vdW) forces instead of covalent ones to maintain the Zn^{2+} coordination geometry in proteins during simulations.[27] For example, the Zn^{2+} vdW parameters in the CHARMM22[28] force field have been derived by first fitting a 12−6 vdW and Coulombic pairwise PEF to the ab initio potential energy hypersurface obtained by Clementi et al.[29] The initial parameters derived from the ab initio calculations (ϵ_{Zn} = 0.67 kcal/mol, σ_{Zn} = 1.70 Å) underestimate the experimental Zn^{2+}−water distance (2.10 ± 0.07 Å)[17] determined from X-ray diffraction studies by 0.14 Å, and overestimate the magnitude of the experimental Zn^{2+} hydration free energy, which ranges from −467[30] to −485[31] kcal/mol by ∼6−10%.[27] Adjusting them to ϵ_{Zn} = 0.25 kcal/mol and σ_{Zn} = 1.95 Å yields a Zn^{2+}−water distance (2.12 Å) and a Zn^{2+} hydration free energy (−473 kcal/mol) that are closer to the respective experimental numbers.[27] However, simulations of Zn-containing proteins such as carbonic anhydrase,[32,33] farnesyltransferase,[34] and phosphotriesterase[35] using the nonbonded model with different sets of Zn^{2+} vdW parameters yield an octahedral or trigonal bipyramidal zinc complex instead of the tetrahedral zinc complex identified in the respective X-ray structures. This discrepancy has been attributed to the Zn^{2+} vdW parameters, which have been parametrized to yield a hexahydrated Zn^{2+} in aqueous solution.[35]

The *semi-bonded* (also known as *cationic dummy atom*) model of Zn−ligand interactions places virtual fractional charges symmetrically around a metal to mimic valence electrons.[36] For example, the problem of a tetrahedral zinc complex converting to an octahedral one in protein simulations can be circumvented by using four cationic dummy atoms to mimic Zn's $4s4p^3$ vacant orbitals, thus imposing the requisite orientational requirement for the ligands.[33] The zinc is assigned *only* vdW parameters, and its +2e charge is evenly distributed among the dummy atoms. Each dummy atom with a charge of 0.5e is tetrahedrally *bonded* to Zn^{2+} and interacts with other atoms in the protein only via *electrostatic* interactions. Simulations of Zn-containing carbonic anhydrase, carboxypeptidase A, rubredoxin, and phosphotriesterase using the *cationic dummy atom* model could maintain the tetracoordination of Zn^{2+} during the entire two nanoseconds (ns) simulation period,[33,35] in contrast to the respective simulations using the nonbonded model (see above). Consequently, it has been suggested that MD simulations using nonbonded Zn−ligand interactions should be used with caution.[35]

Here, we show that, although simulations of proteins with one or more tetracoordinated Zn^{2+} cations using the conventional 12−6 vdW and Coulombic PEF for nonbonded Zn−ligand interactions may not preserve the native metal-binding site structure, the nonbonded model can still yield experimental observables if it includes charge transfer from the ligating atoms to the metal and local polarization of Zn^{2+} and its ligands in conjunction with appropriate vdW parameters for Zn^{2+}. The new PEF and vdW parameters used are described in the next section. They were then used in simulations of (1) a classical Cys_2His_2 Zn-finger domain,[37] in which Zn^{2+} is coordinated to two neutral His and two negatively charged Cys side chains, and (2) a $Zn-Cys_4$ domain,[38] in which Zn^{2+} is bound to four negatively charged Cys.[19] These two types of Zn-finger domains have been chosen because they are ubiquitous modules of protein−nucleic acid and protein−protein recognition.[39] Furthermore, they require Zn^{2+} to fold into the correct three-dimensional structure;[40,41] thus, the CN of Zn^{2+} changes from six in the unfolded state to four in the folded structure. The results show that the new PEF for Zn−water/protein interactions can account for a

(20) Banci, L. *Curr. Opin. Chem. Biol.* **2003**, *7*, 143−149.
(21) Vendani, A.; Huhta, D. W. *J. Am. Chem. Soc.* **1990**, *112*, 4759−4767.
(22) Merz, K. M., Jr. *J. Mol. Biol.* **1990**, *214*, 799−802.
(23) Hoops, S. C.; Anderson, K. W.; Merz, K. M. *J. Am. Chem. Soc.* **1991**, *113*, 8262−8270.
(24) Ryde, U. *Proteins: Struct., Funct., Genet.* **1995**, *21*, 40−56.
(25) Lu, D. S.; Voth, G. A. *Proteins: Struct., Funct., Genet.* **1998**, *33*, 119−134.
(26) Banci, L.; Schroder, S.; Kollman, P. A. *Proteins* **1992**, *13*, 288−305.
(27) Stote, R.; Karplus, M. *Proteins: Struct., Funct., Genet.* **1995**, *23*, 12−31.
(28) MacKerell, J. A. D.; Bashford, D.; Bellott, M.; Dunbrack, R.; Evanseck, J. D.; Field, M. J.; Fischer, S.; Gao, J.; Guo, H.; Ha, S.; Joseph-McCarthy, D.; Kuchnir, L.; Kuczera, K.; Lau, F. T. K.; Mattos, C.; Michnick, S.; Ngo, T.; Nguyen, D. T.; Prodhom, B.; Reiher, W. E. I.; Roux, B.; Schlenkrich, M.; Smith, J. C.; Stote, R.; Straub, J.; Watanabe, M.; Wiorkiewicz-Kuczera, J.; Yin, D.; Karplus, M. *J. Phys. Chem. B* **1998**, *102*, 3586−3616.
(29) Clementi, E.; Corongiu, G.; Jonsson, G.; Romano, S. *J. Chem. Phys.* **1980**, *72*, 260.
(30) Marcus, Y. *Biophys. Chem.* **1994**, *51*, 111−127.
(31) Friedman, H. L.; Krishnan, C. V. *Thermodynamics of ionic hydration*; Plenum Press: New York, 1973; Vol. 3.
(32) Liang, J.-H.; Lipscomb, W. N. *Proc. Natl. Acad. Sci. U.S.A.* **1990**, *87*, 3675−3679.
(33) Pang, Y.-P. *J. Mol. Model.* **1999**, *5*, 196−202.
(34) Pang, Y.-P.; Xu, K.; El Yazal, J.; Prendergast, F. G. *Protein Sci.* **2001**, *9*, 1857−1865.
(35) Pang, Y.-P. *Proteins: Struct., Funct., Genet.* **2001**, *45*, 183−189.
(36) Aqvist, J.; Warshel, A. *J. Mol. Biol.* **1992**, *224*, 7−14.
(37) Elrod-Erickson, M.; Rould, M. A.; Nekludova, L.; Pabo, C. O. *Structure (London)* **1996**, *4*, 1171.
(38) Berry, M. B.; Phillips, G. N. *Proteins: Struct. Funct., Genet.* **1998**, *32*, 276−288.
(39) Wolfe, S. A.; Nekludova, L.; Pabo, C. O. *Annu. Rev. Biophys. Biomol. Struct.* **2000**, *29*, 183-212.
(40) Frankel, A. D.; Berg, J. M.; Pabo, C. O. *Proc. Natl. Acad. Sci. U.S.A.* **1987**, *84*, 4841−4845.
(41) Berg, J. M.; Godwin, H. A. *Annu. Rev. Biophys. Biomol. Struct.* **1997**, *26*, 357−371.

Table 1. Charge Transferred from Atom L to Zn^{2+}, $\Delta q^{eq}_{L\rightarrow Zn}$, at the Equilibrium Zn−L Distance, r^{eq}_{Zn-L}

complex[a]	Atom L	q_{Zn}[b](e)	r^{eq}_{Zn-L} (Å)	$\Delta q^{eq}_{L\rightarrow Zn}$[c](e)
$[Zn(H_2O)_6]^{2+}$	O	1.68	2.12	0.053
$[Zn(CH_3S)_4]^{2-}$	S	1.24	2.44	0.190
$[Zn(CH_3S)_2\ (Im)_2]^0$	N	1.33	2.17	0.145

[a] Geometries fully optimized at the B3-LYP/6-31+G* level. [b] B3-LYP/6-31+G* NBO atomic charges. [c] Charge transferred from atom L to Zn^{2+}, as described in text.

change in the CN of Zn^{2+}: it can reproduce the tetrahedral geometry of the $Zn-Cys_2His_2$ or $Zn-Cys_4$ complex, irrespective of the starting structure.

Methods

Estimating the Ligand→Zn^{2+} Charge Transfer in Equilibrium Zn Complexes. We first estimated the amount of charge transferred from water and the two most common amino acids found bound to Zn^{2+}; viz., His and Cys. This was determined from ab initio calculations of Zn complexes, in which the ligands, His^0 and Cys^-, were modeled by imidazole (Im) and methylthiolate (CH_3S^-), respectively. The geometries of $[Zn(H_2O)_6]^{2+}$, $[Zn(CH_3S)_4]^{2-}$, and $[Zn(CH_3S)_2\ (Im)_2]^0$ were fully optimized at the B3-LYP/6-31+G* level and NBO atomic charges were computed at the same level using the Gaussian 98 program.[42] The B3-LYP/6-31+G* NBO charges on Zn^{2+} in the $[Zn(H_2O)_6]^{2+}$, $[Zn(CH_3S)_4]^{2-}$, and $[Zn(Im)_2(CH_3S)_2]^0$ complexes are 1.68e, 1.24e, and 1.33e, respectively (see Table 1). Assuming that each Zn ligand in the $[Zn(H_2O)_6]^{2+}$ or $[Zn(CH_3S)_4]^{2-}$ complex transfers the same amount of charge to the metal, the charge transferred by a water molecule is $(2 - 1.68)/6 = 0.053$e, while that transferred by a negatively charged CH_3S^- is, as expected, much greater, $(2 - 1.24)/4 = 0.190$e. The charge transferred by an imidazole can then be determined by assuming that CH_3S^- transfers the same amount of charge to Zn^{2+} in the $[Zn(CH_3S)_2(Im)_2]^0$ and $[Zn(CH_3S)_4]^{2-}$ complexes; thus, it is equal to $[(2 - 1.33) - (2 \times 0.19)]/2 = 0.145$e. Thus, the results in Table 1 show that charge transfer from the protein ligands is much greater than that from water molecules and thus should not be neglected in modeling interactions between Zn^{2+} and amino acid residues.

Conventional Potential Energy Function. In the conventional PEF, the interaction energy, $V_{Zn-i}(r)$, between Zn^{2+} and atom, *i*, at any given simulation time-step *t* is modeled by the 12−6 vdW + Coulombic energies:

$$V_{Zn-i}(r) = \sum_i \frac{q_{Zn}q_i}{4\pi\epsilon_0 r_{Zn-i}} + 4\epsilon_{Zn-i}\left[\left(\frac{\sigma_{Zn-i}}{r_{Zn-i}}\right)^{12} - \left(\frac{\sigma_{Zn-i}}{r_{Zn-i}}\right)^{6}\right] \quad (1)$$

In eq 1, q_{Zn} and q_i are respectively the fixed charges on Zn^{2+} (2e) and the *i*th atom, respectively; r_{Zn-i} is the distance between Zn^{2+} and the *i*th atom at time-step *t* during the simulation; ϵ_{Zn-i} and σ_{Zn-i} are vdW parameters obtained using traditional combining rules, $\epsilon_{Zn-i} = (\epsilon_{Zn} \times \epsilon_i)^{1/2}$ and $\sigma_{Zn-i} = (\sigma_{Zn} + \sigma_i)/2$. Because the charge transferred by a water molecule to Zn(II) is negligible (0.053e), the Zn−water interactions could be modeled by eq 1.

New Potential Energy Function. In contrast to water, the amino acid residues, Cys^- and His^0, transfer significant amounts of charge to Zn^{2+} (see Table 1), thus charge transfer and local polarization effects were taken into account in the interaction energy, $V_{Zn-i}(r)$, between Zn^{2+} and atom, *i*, at any given simulation time-step *t*:

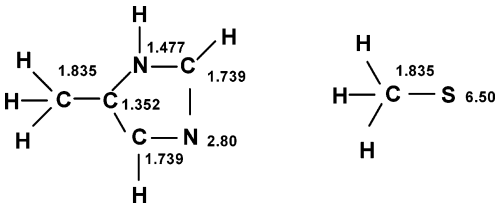

Figure 1. Atomic polarizabilities (Å^3) used in computing the local polarization energy (eq 3).

$$V_{Zn-i}(r) = V^{pol}(r) + \sum_i \frac{q_{Zn}q_i}{4\pi\epsilon_0 r_{Zn-i}} + 4\epsilon_{Zn-i}\left[\left(\frac{\sigma_{Zn-i}}{r_{Zn-i}}\right)^{12} - \left(\frac{\sigma_{Zn-i}}{r_{Zn-i}}\right)^{6}\right] \quad (2)$$

The new PEF in eq 2 differs from the conventional PEF in eq 1 in two ways: First, eq 2 includes an additional electrostatic polarization energy, $V^{pol}(r)$, for Zn^{2+} and all the side-chain atoms of the Zn-bound Cys^-/His^0 residue. Second, eq 2 takes into account the charge transferred by His^0 and/or Cys^- to Zn^{2+}. This is attributed solely to the His(N) and/or Cys(S^-) atoms that are directly coordinated to Zn^{2+} because charge transfer from the other Zn-bound Cys^-/His^0 side-chain atoms, based on the NBO charges of CH_3S^-, Im^0, as compared with those in the $[Zn(CH_3S)_2(Im)_2]^0$ complex, appears to be negligible (<0.05e). Thus, the charges on Zn^{2+} and the S or N atom coordinated to Zn^{2+} in eq 2 are *not* fixed but change during the simulation, depending on the interatomic distance between Zn^{2+} and the S/N atom, $r_{Zn-S/N}$, at time-step *t* (see below). The charges on the other atoms that are not directly bonded to Zn^{2+} do not change during the simulation.

Computing the Polarization Energy. The local polarization energy at each time-step *t*, $V^{pol}(r)$, was computed according to:

$$V^{pol}(r) = -\frac{1}{2}\sum_i \mu_i E_i^0 \quad (3)$$

where the summation is over Zn and all the side-chain atoms of each Zn-bound residue, μ_i is the dipole induced on atom *i*, and $\boldsymbol{E}_i^0$ is the electrostatic field produced by the current charges at the *i*th polarizable site. The induced dipole moment is proportional to the total electrostatic field, $\boldsymbol{E}_i$:

$$\mu_i = \alpha_i E_i \quad (4)$$

where the proportionality constant, α_i, is the polarizability of the *i*th atom. The atomic polarizabilities used are shown in Figure 1. The polarizabilities of the ligating His(N) and Cys(S^-) were empirically adjusted to reproduce the experimental distances to Zn^{2+} in the Cys_2-His_2 Zn-binding site, whereas those of the remaining side-chain atoms in Figure 1 are optimized atomic hybrid polarizabilities taken from ref 43, while the Zn^{2+} polarizability, 2.294 Å^3, is taken from ref 44. The total electric field at the Zn atom, $\boldsymbol{E}_{Zn}$, is the vector sum of the field due to the current charges and induced dipoles of the Zn ligand atoms *j*; i.e.,

$$E_{Zn} = E_{Zn}^0 + \sum_j T_{Zn-j}\mu_j = \sum_j \frac{q_j \vec{r}_{Zn-j}}{r_{Zn-j}^3} + \sum_j \frac{\vec{\mu}_j}{r_{Zn-j}^3}\left(\frac{3\vec{r}_{Zn-j}\vec{r}_{Zn-j}}{r_{Zn-j}^2} - 1\right) \quad (5a)$$

In eq 5a, the summation is over all the side-chain atoms of each Zn-

(42) Frisch, M. J.; Trucks, G. W.; Schlegel, H. B.; Scuseria, G. E.; Robb, M. A.; Cheeseman, J. R.; Zakrzewski, V. G.; Montgomery, J. A., Jr.; Stratmann, R. E.; Burant, J. C.; Dapprich, S.; Millam, J. M.; Daniels, A. D.; Kudin, M. C.; Strain, K. N.; Farkas, O.; Tomasi, J.; Barone, V.; Cossi, M.; Cammi, R.; Mennucci, B.; Pomelli, C.; Adamo, C.; Clifford, S.; Ochterski, J.; Petersson, G. A.; Ayala, P. Y.; Cui, Q.; Morokuma, K.; Malick, D. K.; Rabuck, A. D.; Raghavachari, K.; Foresman, J. B.; Cioslowski, J.; Ortiz, J. V.; Stefanov, B. B.; Liu, G.; Liashenko, A.; Piskorz, P.; Komaromi, I.; Gomperts, R.; Martin, R. L.; Fox, D. J.; Keith, T.; Al-Laham, M. A.; Peng, C. Y.; Nanayakkara, A.; Gonzalez, C.; Challacombe, M.; Gill, P. M. W.; Johnson, B.; Chen, W.; Wong, M. W.; Andres, J. L.; Gonzalez, C.; Head-Gordon, M.; Replogle, E. S.; Pople, J. A. *Gaussian 98*, revision A.5,; Gaussian, Inc.: Pittsburgh, 1998.

(43) Miller, K. J. *J. Am. Chem. Soc.* **1990**, *112*, 8533−8542.

(44) Johnson, W. R.; Kolb, D.; Huang, K.-N. *At. Mol. Nucl. Data Tables* **1983**, *28*, 333.

bound residue. On the other hand, the total electric field $\boldsymbol{E}_i$ at a Zn-bound amino acid side-chain atom i is the sum of the field due to the Zn charge and its induced dipole; i.e.,

$$E_i = \frac{q_{Zn}\vec{r}_{i-Zn}}{r^3_{i-Zn}} + \frac{\vec{\mu}_{Zn}}{r^3_{i-Zn}}\left(\frac{3\vec{r}_{i-Zn}\vec{r}_{i-Zn}}{r^2_{i-Zn}} - 1\right) \quad (5b)$$

Thus,

$$\mu_i(t) = \alpha_i E_i^0 + \alpha_i \sum_{j\neq i} T_{ij}\mu_j \quad (6)$$

is obtained by solving a set of coupled equations iteratively. To avoid unphysical growth of the induced dipoles at close distances to each other and to the permanent electric charges, we introduced a cutoff distance, r_{ij}^{cutoff}, which is assumed to be equal to the sum of the vdW radii of atoms i and j scaled by a parameter γ (= 0.92),[45] for small interatomic distances r_{ij} such that $r_{ij} = r_{ij}^{cutoff}$ if $r_{ij} \leq r_{ij}^{cutoff}$.

Estimating the Distance-Dependent Charges on Zn, S(Cys$^-$), and N(His^0). The amount of charge transferred from the ligand atom L to Zn^{2+}, $\Delta q_{L\rightarrow Zn}$, clearly depends on their interatomic distance, r_{Zn-L}, at any given time-step t during the simulation. At the equilibrium r^{eq}_{Zn-L} distance, the charge transferred by a ligand was attributed to the atom ligating to Zn^{2+} (see above and Table 1). At a distance greater than the sum of the vdW radii of Zn^{2+} and the ligating atom, the charge transferred by the ligating atom to the metal would be expected to be negligible. Thus, assuming a linear dependence of the amount of charge transfer on the r_{Zn-L} distance, the charge transferred from atom L to Zn^{2+} at a given simulation time-step, $\Delta q_{L\rightarrow Zn}$, can be estimated from:

$$\Delta q_{L\rightarrow Zn} = a_L \times r_{Zn-L} + b_L \quad (7)$$

$b_S = 0.91$e and $a_S = -0.297$ e/Å, while $b_N = 0.71$e and $a_N = -0.26$e/Å based on the equilibrium r^{eq}_{Zn-L} distances and $\Delta q^{eq}_{L\rightarrow Zn}$ values in Table 1, as well as the vdW radii in the CHARMM22 force field.[28]

The charge on S(Cys$^-$) or N(His^0) at each time-step t in the simulation can thus be computed from:

$$q_L = q_L^{CHARMM} + \Delta q_{L\rightarrow Zn} \quad (8)$$

where the CHARMM charge on S(Cys$^-$), q_S^{CHARMM}, equals -0.80e, while that on N(His^0), q_N^{CHARMM}, equals -0.70e.[28] At the equilibrium r^{eq}_{Zn-S} distance, eq 8 yields $q_S = -0.80\text{e} + 0.19\text{e} = -0.61$e, which is in excellent agreement with the respective NBO charge on S of -0.61e in the B3-LYP/6-31+G* fully optimized $[Zn(CH_3S)_2(Im)_2]^0$ complex. On the other hand, at the equilibrium r^{eq}_{Zn-N} distance, eq 8 yields $q_N = -0.70\text{e} + 0.145\text{e} = -0.555$e, which slightly underestimates the respective NBO charge on N of -0.626e in the fully optimized $[Zn(CH_3S)_2(Im)_2]^0$ complex. At any given simulation time-step, the charge on Zn, q_{Zn}, can be computed from the total charge transferred by all the ligands to Zn^{2+}, ΔQ:

$$q_{Zn} = 2 - \Delta Q \quad (9)$$

Calculations

MD simulations were carried out at physiological pH and a mean temperature of 300 K using a modified CHARMM27 program[46] on (1) a 33 amino acid $Zn-Cys_2His_2$ peptide containing 548 atoms solvated with 2638 water molecules and (2) a 34 amino acid $Zn-Cys_4$ peptide containing 533 atoms solvated with 1872 water molecules.

Table 2. Zn^{2+} vdW Parameters Used in the Simulations

set	ϵ_{Zn} kcal/mol	σ_{Zn} Å
A	0.183	1.57
B	0.250[a]	1.95[a]
C	0.670[a]	1.70[a]

[a] Taken from Stote & Karplus.[27]

Force Field. For each Zn−peptide, MD simulations were performed using the three Zn^{2+} parameter sets listed in Table 2. In set C, ϵ_{Zn} and σ_{Zn} were obtained from fitting to an ab initio-derived Zn−water potential energy surface[29] (see Introduction). Set B differs from set C in tuning the ϵ_{Zn} and σ_{Zn} parameters in set C so as to reproduce the experimental first-shell Zn−O(water) distance, the Zn^{2+} CN of six in water, and the *absolute* Zn^{2+} hydration free energy (see Introduction).[27] Note that the parameters in set B correspond to those in the CHARMM22 force field.[28] The parameters in set A were derived from those in set B by adjusting them to reproduce the experimental first and second-shell Zn^{2+}−O(water) distances and CNs, as well as the experimental hydration free energy of Zn^{2+} *relative* to the experimental hydration free energies of other metal dications.[47] For all three Zn^{2+} parameter sets, the vdW parameters of the Zn-bound S^- ($\epsilon_S = 0.47$ kcal/mol; $\sigma_S = 3.92$ Å) and N ($\epsilon_N = 0.20$ kcal/mol; $\sigma_N = 3.30$ Å) were taken from the CHARMM22 force field.[28,48]

All the simulations employed the TIP3P model for water molecules[49] and the CHARMM22 parameters[28] for the protein atoms, unless stated otherwise. The simulations were carried out at neutral pH, therefore all Asp and Glu as well as the Zn-bound His and Cys were deprotonated, whereas all Lys, Arg, and His that are not bound to Zn^{2+} were protonated. The charge assignment resulted in a net charge of 3e for the $Zn-Cys_2His_2$ peptide and a neutral $Zn-Cys_4$ peptide. Bonds involving hydrogen atoms were constrained during the simulations using the SHAKE algorithm.[50] The vdW energies and electrostatic forces were switched at a distance of 9.5 Å to zero at 11.5 Å by atom-based energy-switching and force-switching functions, respectively. The nonbonded interaction list was updated every five steps using a cutoff of 12.5 Å. The Zn protein simulations used periodic boundary conditions with a truncated octahedral primary simulation box[51] of edge length equal to 27.5 and 25.0 Å for the $Zn-Cys_2His_2$ and $Zn-Cys_4$ systems, respectively.

Simulation Protocol. The starting point for the *classical* Zn-finger peptide simulations is the 1.6 Å X-ray structure of the Zif268 Zn-finger DNA complex (PDB entry 1AAY, amino acids 103−135 corresponding to the classical Zn-finger domain), whereas that for the $Zn-Cys_4$ simulations is the 1.6 Å X-ray structure of the adenylate kinase (PDB entry 1ZIN, amino acids 127−160 corresponding to the active site lid domain). After placing hydrogen atom positions using the HBUILD facility in CHARMM, the hydrogen-built structure was first energy minimized in the presence of strong harmonic constraints on all heavy atoms to relieve close vdW contacts and strained bond angles. The resulting structure was immersed in the center of a

(45) Kaminski, G. A.; Jorgensen, W. L. *J. Chem. Soc., Perkin Trans. 2* **1999**, 2365−2375.
(46) Brooks, B. R.; Bruccoleri, R. E.; Olafson, B. D.; States, D. J.; Swaminathan, S.; Karplus, M. *J. Comput. Chem.* **1983**, *4*, 187−217.
(47) Babu, C. S.; Lim, C. **2004**, *in preparation*.
(48) Wang, J.; Xiang, Y.-F.; Lim, C. *Prot. Engng.* **1994**, *7*, 75−82.
(49) Jorgensen, W. L.; Chandrasekhar, J.; Madura, J. D.; Impey, R. W.; Klein, M. L. *J. Chem. Phys.* **1983**, *79*, 926−923.
(50) Ryckaert, J. P.; Ciccotti, G.; Berendsen, H. J. C. *J. Comput. Phys.* **1977**, *23*, 327.
(51) Allen, M. P.; Tildesley, D. J. *Computer Simulation of Liquids*; Oxford University Press: New York, 1990.

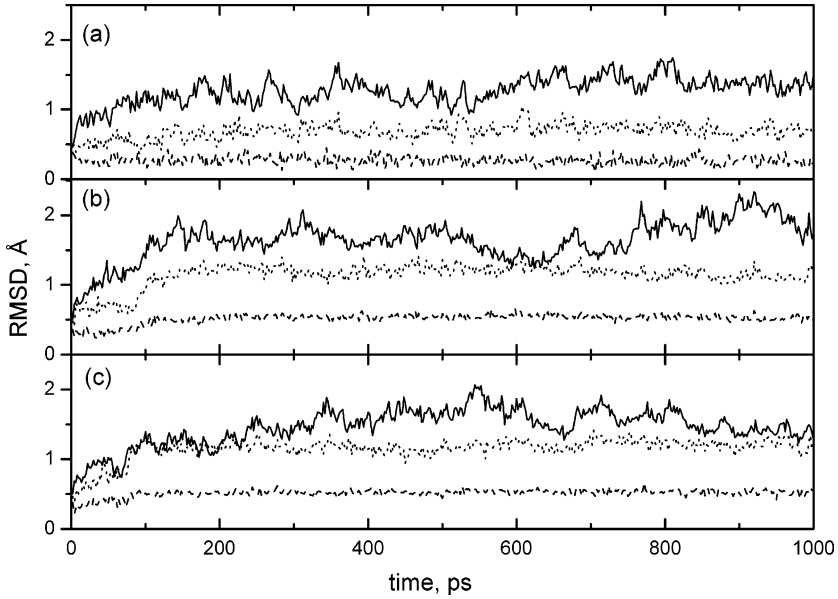

Figure 2. RMSDs of the protein backbone (solid curves), Zn−Cys_2His_2 complex (dotted curves), as well as Zn−S(Cys^-)/N(His^0) (dashed curves) from the starting X-ray structure (PDB entry 1AAY) during the Cys_2His_2 Zn-finger simulation using (a) the new PEF (eq 2) with parameter set A, (b) the conventional 12−6 vdW + Coulombic PEF (eq 1) with parameter set B, and (c) eq 1 with parameter set C.

previously equilibrated truncated octahedral box of TIP3P water molecules of density ~1 g/cm^3, and its orientation in the primary box was optimized to ensure sufficient solvation of all parts of the protein.[52] Water molecules whose oxygen atoms were within 2.5 Å of any protein heavy atom were deleted. The resulting structure was subjected to several steps of minimization using steepest descent followed by adopted-basis Newton Raphson with strong harmonic constraints on all heavy atoms. All the atoms were then propagated according to Newton's equations of motions using the leapfrog Verlet algorithm with a time step of 2×10^{-15} s at a mean temperature of 300 K. The solvated protein was then equilibrated for 200 ps, followed by 800 ps of production dynamics. The total energy and temperature remained *constant* (within 0.1% and ±4 K, respectively) during each simulation.

Zn−Cys_2His_2 Peptide Simulation Results

Three 1-ns simulations of a classical Cys_2His_2 Zn-finger peptide starting from the same X-ray configuration (denoted by the subscript X) were carried out. The first simulation, referred to as $2A_X$, is based on the new PEF (eq 2), which includes both charge transfer and local polarization effects, using parameter set A (Table 2). The other two simulations, referred to as $1B_X$ and $1C_X$, are based on the conventional 12−6 vdW + Coulombic PEF (eq 1) using parameter sets B and C, respectively. For all three classical Zn-finger simulations, the root-mean-square deviation (RMSD) of the backbone heavy atoms from those in the starting X-ray structure (Figure 2, solid curves) initially rose, then plateaued after ~200 ps, and fluctuated around a mean of 1.32 ± 0.16 Å in simulation $2A_X$ (Figure 2a), and around a higher mean of 1.71 ± 0.22 Å in simulation $1B_X$ (Figure 2b) and 1.56 ± 0.17 Å in simulation $1C_X$ (Figure 2c). Thus, the first 200 ps of each trajectory were excluded, while the remaining 800 ps were used in computing the average structures, distances, and angles.

Interestingly, the RMSDs in simulation $2A_X$ are consistently lower than those in simulations $1B_X$ and $1C_X$, suggesting that the inclusion of charge transfer and local polarization effects help to stabilize the metal-binding site and overall structure. Besides the protein backbone RMSD, the RMSD of Zn^{2+} and its direct ligands, Cys^- and His^0, (Figure 2, dotted curves) fluctuated around a mean of 0.72 ± 0.09 Å in simulation $2A_X$, which is lower than that in simulation $1B_X$ or $1C_X$ (1.19 ± 0.08 Å). Furthermore, the RMSD of Zn^{2+}, S(Cys^-), and N(His^0) (Figure 2, dashed line) fluctuated around a mean of 0.27 ± 0.06 Å in simulation $2A_X$, which is also lower than that in simulation $1B_X$ (0.54 ± 0.03 Å) or $1C_X$ (0.53 ± 0.03 Å). The smaller RMSD of Zn^{2+} and its ligands, as compared to the backbone RMSD, indicate that the metal-binding site is significantly more rigid than the rest of the protein.

The Conventional PEF Yields a Nontetrahedral Zn−Cys_2His_2 Binding Site. Another indication that inclusion of charge transfer and local polarization effects help to maintain structural integrity is illustrated in Figure 3, which shows the crystal structure of the Cys_2His_2 Zn-finger domain superimposed upon the average MD structures derived from the three simulations. In the X-ray structure, Zn^{2+} is tetracoordinated to two negatively charged cysteines (Cys^{107} and Cys^{112}) in a β-hairpin and two neutral histidines (His^{125} and His^{129}) in the C-terminal portion of the α-helix. The tetracoordination geometry of Zn^{2+} is maintained during the entire $2A_X$ simulation (Figure 3a). This finding together with the relatively low RMSDs from the X-ray structure (see above and Figure 2a) indicates that the new PEF (eq 2) with parameter set A can maintain the structural integrity of the Zn−Cys_2His_2 peptide.

In contrast to simulation $2A_X$, the average structures derived from simulations $1B_X$ and $1C_X$ show Zn^{2+} *hexacoordinated* to two Cys^-, two His^0, and two water molecules (Figures 3b and 3c). Because the loop connecting the two β-strands is significantly distorted from the respective X-ray conformation, the conformation of the Cys^{112} side chain, which is located in the loop, exhibits the greatest deviation from that in the X-ray

(52) Mezei, M. *J. Comput. Chem.* **1997**, *18*, 812−815.

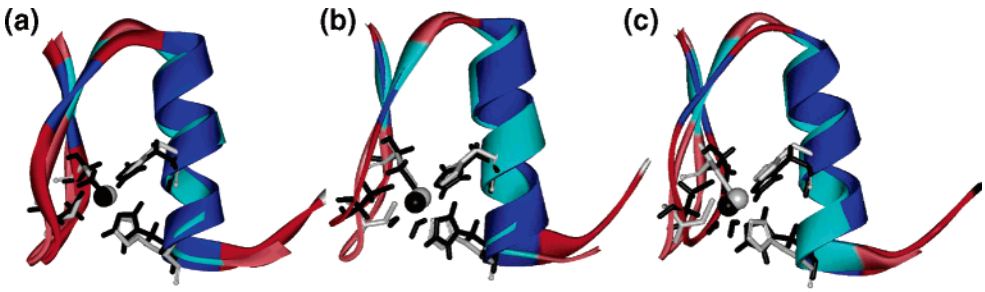

Figure 3. Crystal structure (light color) of the Zif268 Cys_2His_2 Zn-finger domain superimposed upon the average MD structure (dark color) derived from simulations using (a) the new PEF (eq 2) with parameter set A, (b) the conventional 12−6 vdW + Coulombic PEF (eq 1) with parameter set B, and (c) eq 1 with parameter set C. The metal-binding site is in black (MD) or gray (X-ray), while the regular secondary structures are in dark blue (MD) and light blue (X-ray), whereas the loops are in red (MD) and pink (X-ray).

Table 3. Comparison between MD and Experimental CNs and Average Zn Angles and Distances in the Zif268 Zn-Finger Peptide

method	V^{pol}+CT[a]	CN	S–Zn–S (deg)	N–Zn–N (deg)	Zn–S (Å)	Zn–N (Å)
X-ray[b]		4	117 ± 6	105 ± 6	2.29 ± 0.10	2.04 ± 0.08
MD-$2A_X$[c,d]	yes	4	136 ± 8	95 ± 5	2.31 ± 0.05	2.04 ± 0.06
MD-$1B_X$[c,e]	no	6	104 ± 5	86 ± 4	2.59 ± 0.08	2.25 ± 0.08
MD-$1C_X$[c,f]	no	6	103 ± 4	87 ± 4	2.57 ± 0.08	2.22 ± 0.07
MD-$2A_B$[g,d]	yes	4	137 ± 11	95 ± 7	2.33 ± 0.06	2.04 ± 0.06
MD-$1A_B$[g,h]	no	6	96 ± 5	88 ± 4	2.55 ± 0.13	2.11 ± 0.05
MD-$2B_B$[g,i]	yes	6	104 ± 5	82 ± 4	2.58 ± 0.07	2.30 ± 0.09
MD-$2C_B$[g,j]	yes	6	112 ± 15	85 ± 4	2.53 ± 0.05	2.24 ± 0.05

[a] "yes" means charge transfer (CT) and polarization energy (V^{pol}) are included in the PEF, whereas "no" means that they are not included in the PEF. [b] Mean values and standard deviations obtained by averaging over the three zinc-finger binding sites from PDB entry 1AAY. [c] Starting from the X-ray structure. [d] Using eq 2 and set A parameters from Table 2. [e] Using eq 1 and set B parameters from Table 2. [f] Using eq 1 and set C parameters from Table 2. [g] Starting from the end-point of simulation $1B_X$. [h] Using eq 1 and set A parameters from Table 2. [i] Using eq 2 and set B parameters from Table 2. [j] Using eq 2 and set C parameters from Table 2.

structure. The nontetrahedral Zn-binding site together with the relatively high RMSDs from the X-ray structure (Figures 2b and 2c) indicates that the conventional PEF (eq 1) cannot faithfully reproduce the experimentally observed Zn−Cys_2His_2 binding site geometry and overall structure.

The different Zn^{2+} coordination geometries found with the different PEFs and Zn^{2+} vdW parameters are also evident from the Zn^{2+} angles and distances averaged over each of the trajectories (Table 3). The repulsion between the two negatively charged Cys side chains and the larger vdW radius of S (σ_S = 3.92 Å), as compared to that of N (σ_N = 3.30 Å), probably cause the S−Zn−S angle to be larger than the N−Zn−N angle in the X-ray structure, resulting in a distorted tetrahedral Zn complex. Simulation $2A_X$ yields average S−Zn−S and N−Zn−N angles as well as average Zn−S(Cys^-) and Zn−N(His^0) distances that are close to those found in the three zinc-finger binding sites in the crystal structure. In contrast, simulations $1B_X$ and $1C_X$ both underestimate the average X-ray S−Zn−S (by ∼14°) and N−Zn−N angles (by ∼19°), while they overestimate the average X-ray Zn−S (by ∼0.3 Å) and Zn−N distances (by ∼0.2 Å). They yield three near-linear angles (the average value of the S^{107}−Zn−O, S^{112}−Zn−N,[129] and N^{125}−Zn−O angles is 168 ± 4° in simulation $1B_X$ and 169 ± 4° in simulation $1C_X$), whereas the average of the other angles about Zn is 90 ± 4°, indicative of an octahedral (as opposed to a tetrahedral) structure.

The New PEF and Parameters Reproduce the Experimental Zn−Cys_2His_2 Geometry, Irrespective of the Starting Structure. To check if the new PEF can yield a tetrahedral Zn-binding site from an initial nontetrahedral Zn^{2+} configuration, we carried out a simulation using the new PEF (eq 2) and parameter set A starting from the end-point of simulation $1B_X$ (referred to as $2A_B$). After ∼150 ps in simulation $2A_B$, both Zn−O(water) distances in the initial *hexa*coordinated Zn complex increased from 2.1 Å to more than 5 Å, yielding a *tetra*coordinated Zn complex. The structure averaged over the last 150 ps shows that the Zn-binding site structure agrees with the respective crystal structure: The average S−Zn−S and N−Zn−N angles as well as the average Zn−S and Zn−N distances derived from simulation $2A_B$ are similar to those derived from simulation $2A_X$, and are close to the respective X-ray values (Table 3, MD-$2A_B$). These results suggest that simulations using the new PEF (eq 2) with parameter set A can reproduce the observed geometry of the Zn−Cys_2His_2 binding site, irrespective of the starting structure.

Which Forces are Responsible for the Structural Integrity of the Zn−Cys_2His_2 Binding Site? Simulation $2A_X$, which yields a *tetra*coordinated Zn, differs from simulations $1B_X$ and $1C_X$, which yield a *hexa*coordinated Zn, in three ways. The first is the inclusion of charge transfer from the Zn-ligating atoms, S(Cys^-) and N(His^0), to the metal. The second is the addition of the polarization energy of Zn^{2+} and its ligands. The third is the use of smaller $|\epsilon_{Zn}|$ and σ_{Zn} vdW parameters. To reveal the factors responsible for the observed change in the Zn^{2+} CN in simulations with the conventional PEF, we carried out additional simulations starting from the end-point of simulation $1B_X$ (denoted by the subscript B). Simulation $1A_B$ is based on the conventional PEF (eq 1) with parameter set A, while simulations $2B_B$ and $2C_B$ employ the new PEF (eq 2) but with parameter sets B and C, respectively.

In contrast to simulation $\mathbf{2}A_B$, when charge transfer and local polarization effects are omitted from the new PEF in simulation $1A_B$, the initial hexacoodinated Zn^{2+} *cannot* convert to a tetrahedral structure. The structure averaged over the last 200 ps of simulation $1A_B$ shows Zn^{2+} *hexa*coordinated to two Cys^-, two His^0, and two water molecules. This is partly because the full +2e charge on Zn in simulation $1A_B$ attracts water molecules to the metal. Furthermore, the average Zn−S and Zn−N distances derived from simulation $1A_B$ are greater than those derived from simulation $\mathbf{2}A_B$ (by 0.22 and 0.07 Å, respectively), whereas the average Zn−N distance is slightly shorter than that derived from simulation $\mathbf{1}B_B$ (by 0.14 Å, see Table 3). Thus, the difference between the results of simulations $\mathbf{1}A_B$ and $\mathbf{2}A_B$ highlights the importance of charge transfer and local polarization effects in maintaining the correct coordination geometry of the Zn−Cys_2His_2 binding site.

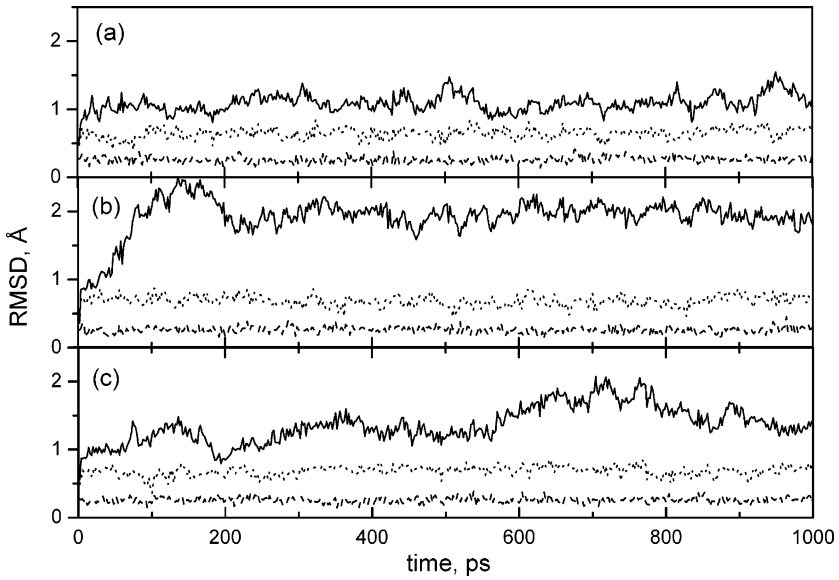

Figure 4. RMSDs of the protein backbone (solid curves), Zn−Cys_4 complex (dotted curves), and Zn−S(Cys^-) (dashed curves) from the starting X-ray structure (PDB entry 1ZIN) during the Zn−Cys_4 peptide simulation using (a) eq 2 with parameter set A, (b) eq 1 with parameter set B, and (c) eq 1 with parameter set C.

Charge transfer and local polarization effects, however, do not suffice to maintain the structural integrity of the Zn−Cys_2-His_2 binding site in the X-ray structure. This is evidenced by comparing the results of simulations **2**B_B and **2**C_B with those of simulations **1**B_X and **1**C_X, respectively, where adding charge transfer and local polarization effects to the conventional PEF using set B or C Zn^{2+} vdW parameters *cannot* convert the initial hexacoordinated Zn^{2+} to a tetrahedral one, in contrast to simulation **2**A_B (see above). Starting from the end-point of simulation **1**B_X, Zn^{2+} remains *octahedrally* coordinated to two Cys^-, two His^0, and two water molecules throughout the 400-ps trajectory in simulation **2**B_B or **2**C_B.

In addition to charge transfer and local polarization effects, appropriate vdW parameters for Zn^{2+} are also important in attaining the correct Zn^{2+} coordination geometry, as evidenced from comparing the results of simulation 2**B**$_B$/2**C**$_B$ with those of simulation 2**A**$_B$. Relative to simulation 2**A**$_B$, increasing the magnitude of the Zn^{2+} vdW parameters in simulation 2**B**$_B$ or 2**C**$_B$ elongates the Zn−S and Zn−N distances by more than 0.20 Å (compare MD-2**B**$_B$ and MD-2**C**$_B$ with MD-2**A**$_B$ in Table 3). The increase in the Zn−S and Zn−N distances decreases the amount of charge transferred by the protein ligands to Zn (see eq 7) and increases the average Zn charge in simulation 2**B**$_B$ (1.48e) or 2**C**$_B$ (1.42e) relative to that in simulation 2**A**$_B$ (1.20e). This enhances Zn−water electrostatic interactions to such an extent that the water molecules remain bound to the metal.

Note that including charge transfer effects and changing only the Zn^{2+} vdW parameters would not be sufficient to reproduce the experimentally observed Zn−Cys_2His_2 binding site. This is because charge transfer reduces the magnitudes of the partial charges on zinc, S(Cys^-) and N(His^0), which, in turn, attenuates the $Zn^{\delta+}$−Cys^-/His^0 electrostatic charge−charge/dipole interactions. Including local polarization energy of Zn^{2+} and its ligands, which also depend on the partial charges, compensates for the decreased $Zn^{\delta+}$−Cys^-/His^0 electrostatic interactions.

In summary, the results of simulations 2A_B, 1A_B, 2B_B, and 2C_B show that all three factors; viz., charge transfer, local polarization, and appropriate Zn^{2+} vdW parameters, appear to be important in maintaining the structural integrity of the Zn−Cys_2His_2 binding site.

Zn−Cys_4 Peptide Simulation Results

As for the Zn−Cys_2His_2 simulations, three 1-ns simulations of the Zn−Cys_4 adenylate kinase lid domain starting from the same X-ray configuration were carried out using the new PEF (eq 2) with parameter set A (2A_X) as well as the conventional PEF (eq 1) with parameter sets B (1B_X) and C (1C_X). After ∼200 ps, the RMSD of the protein backbone from the starting X-ray structure (Figure 4, solid curves) fluctuated around a mean of 1.11 ± 0.12 Å in simulation 2A_X (Figure 4a), and around a much higher mean of 1.95 ± 0.12 Å in simulation 1B_X (Figure 4b) and 1.43 ± 0.24 Å in simulation 1C_X (Figure 4c). As in the Zn−Cys_2His_2 simulations, the first 200 ps of each trajectory were excluded and the last 800 ps were used in computing the average structures, distances, and angles (see below).

In contrast to the Zn−Cys_2His_2 simulations, all three different force fields seem to be comparable in stabilizing the metal-binding site as the RMSDs of the Zn−Cys_4 complex and Zn−S(Cys) are similar. In simulations 2A_X, 1B_X, and 1C_X, the RMSDs of the four Cys^- and Zn^{2+} fluctuated around a mean of 0.65 ± 0.07 Å, 0.68 ± 0.08 Å, and 0.69 ± 0.06 Å, respectively (Figure 4, dotted curve), while the RMSDs of the four S(Cys^-) atoms and Zn^{2+} fluctuated around a mean of 0.26 ± 0.05 Å, 0.26 ± 0.05 Å, and 0.26 ± 0.04 Å, respectively (dashed curve).

Both New and Conventional PEFs Yield a Tetrahedral Zn−Cys_4 Binding Site. Another indication that all three different force fields appear comparable in stabilizing the metal-binding site is illustrated in Figure 5, which shows the crystal structure of the Zn−Cys_4 adenylate kinase lid domain superimposed upon the average MD structures derived from the three simulations. In the X-ray structure, Zn^{2+} is tetrahedrally coordinated to four Cys^- with an average S−Zn−S angle of 107 ± 5° and an average Zn−S distance of 2.32 ± 0.02 Å (Table 4). The tetrahedral geometry of Zn^{2+} is maintained

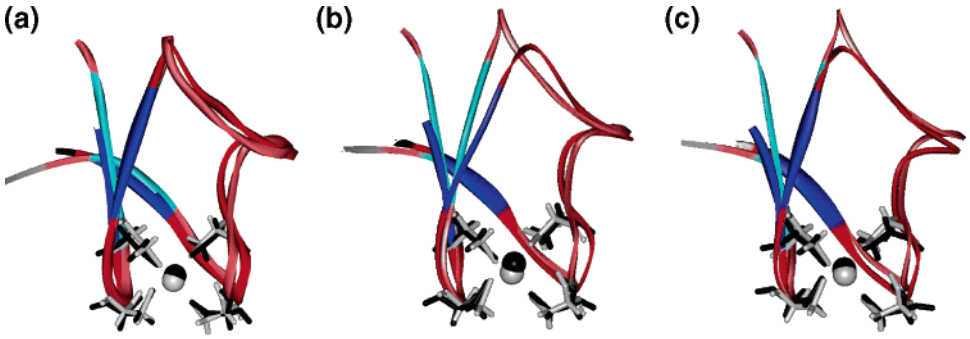

Figure 5. Crystal structure of the Zn−Cys_4 adenylate kinase lid domain superimposed upon the average MD structure derived from simulations using (a) eq 2 with parameter set A, (b) eq 1 with parameter set B, and (c) eq 1 with parameter set C. The metal-binding site is in black (MD) or gray (X-ray), while the regular secondary structures are in dark blue (MD) and light blue (X-ray), whereas the loops are in red (MD) and pink (X-ray).

Table 4. Comparison between MD and Experimental CNs and Average Zn Angles and Distances in the Zn−Cys_4 Adenylate Kinase Lid Domain

method	CN	S–Zn–S (deg)	Zn–S^{130} (Å)	Zn–S^{133} (Å)	Zn–S^{150} (Å)	Zn–S^{153} (Å)
X-ray[a]	4	107 ± 5	2.34 ± 0.01	2.30 ± 0.01	2.32 ± 0.01	2.33 ± 0.01
MD-$2A_X$[b,c]	4	107 ± 5	2.37 ± 0.06	2.41 ± 0.07	2.38 ± 0.06	2.43 ± 0.07
MD-$1B_X$[b,d]	4	107 ± 5	2.42 ± 0.05	2.45 ± 0.05	2.42 ± 0.05	2.46 ± 0.06
MD-$1C_X$[b,e]	4	107 ± 5	2.41 ± 0.05	2.44 ± 0.05	2.41 ± 0.05	2.46 ± 0.05

[a] Residue number corresponds to that in the X-ray structure; values from PDB entry 1ZIN. [b] Starting from the X-ray structure. [c] Using eq 2 and set A parameters from Table 2. [d] Using eq 1 and set B parameters from Table 2. [e] Using eq 1 and set C parameters from Table 2.

throughout the one ns simulations with the new PEF as well as with the conventional force fields (Figures 5a-5c). However, in the average dynamics structure derived from simulation $1B_X$ and $1C_X$ (Figures 5b and 5c), the loops/β-turns are significantly distorted from the respective X-ray conformation, consistent with the larger RMSDs of the *protein backbone* found in these two simulations (see above).

The greater deviations of the overall structure derived from simulations $1B_X$ and $1C_X$ correlate with the greater deviations of the Zn−S distances in these two simulations. Both simulations $1B_X$ and $1C_X$ using the conventional PEF yield average Zn−S distances ranging from 2.41 to 2.46 Å, which overestimate the corresponding average X-ray values by 0.07−0.15 Å. In contrast, simulation $2A_X$ with the new PEF yields average Zn−S distances (2.37−2.43 Å) that are closer to the observed values (Table 4). Thus, the new PEF with parameter set A seems to reproduce the X-ray structure of the Zn−Cys_4 complex better than the conventional PEF with either parameter set B or C.

Discussion

In this work, we have developed a novel PEF for protein simulations of Zn^{2+} bound to Cys^- and/or His^0. The new PEF (eq 2) differs from the conventional PEF (eq 1) in taking into account charge transfer from the ligands to Zn^{2+} and electrostatic polarization of Zn^{2+} and its ligands. Although the charges on Zn^{2+} and its ligating atoms as well as the local polarization energy are evaluated at each time-step in the simulation, the computations are simple and fast and the CPU cost with the new PEF is only 1.11% greater than that with the conventional PEF. Thus, simulations with the PEF will be computationally less expensive than QM/MM simulations with a quantum mechanical description of the zinc core.

Besides introducing a new PEF (eq 2), the vdW parameters for Zn^{2+} also differ from those in the widely used CHARMM22 force field. Notably, the ϵ_{Zn} (0.18 kcal/mol) and σ_{Zn} (1.57 Å) are smaller than the respective CHARMM values (0.25 kcal/mol and 1.95 Å, see Table 2). Another difference is that the new Zn^{2+} vdW parameters reproduce the experimental hydration free energy of Zn^{2+} *relative* to a series of divalent metal cations,[47] whereas the CHARMM22 Zn^{2+} vdW parameters reproduce the *absolute* experimental hydration free energy of Zn^{2+}, which is less certain than the *relative* experimental hydration free energies.

The New PEF is Useful in Simulations in which Zn^{2+} Undergoes a Change in CN/Geometry. The new PEF and parameter set A (Table 2) can account for the change in the Zn^{2+} CN upon binding Cys^- and His^0, which occurs in the Zn-induced folding of Zn-finger peptides and in certain enzymatic reactions. This is evidenced by the ability of the new PEF and parameter set A to faithfully reproduce the overall protein X-ray structure, in particular the tetrahedral structure of the Zn−Cys_2-His_2 binding site, independent of the starting structure (Table 3, MD-$2A_X$ and MD-$2A_B$). Interestingly, the new PEF and parameter set A could reproduce the X-ray structures of the Zn−Cys_2His_2 and Zn−Cys_4 binding sites without introducing many-body forces or having to further adjust vdW parameters of the metal or the ligand atoms (see below).

The Conventional PEF Yields a Nontetrahedral Zn−Cys_2His_2 but a Tetrahedral Zn−Cys_4 Binding Site. In contrast to the new PEF with parameter set A, the conventional PEF (eq 1) with CHARMM parameters (set B in Table 2) yield an *octahedrally* coordinated Zn^{2+} in classical Cys_2His_2 Zn-finger proteins, as in aqueous solution. However, both the new and conventional PEFs can preserve the tetrahedral Zn-Cys_4 geometry observed in the X-ray structure of the adenylate kinase lid domain. The finding that the conventional PEF can preserve the local Zn−Cys_4 geometry is consistent with previous works. Simulations have been carried out on the glucocorticoid receptor DNA-binding domain containing two Zn−Cys_4 binding sites using the conventional PEF with CHARMM22 Zn^{2+} vdW parameters.[53] However, to reproduce the tetrahedral geometry of the Zn-binding site, the vdW parameters and the charges on the S(Cys^-) and C^β atoms had to be adjusted from the CHARMM22 values. The charge on S(Cys^-) was fixed at −0.65e, while ϵ_S and σ_S were increased from the CHARMM values of 0.47 kcal/mol and 3.92 Å to 0.92 kcal/mol and 4.02 Å, respectively. Since the conventional PEF with CHARMM parameters yields a tetrahedral Zn−Cys_4 complex, the conver-

(53) Bredenberg, J.; Nilsson, L. *Int. J. Quantum Chem.* **2001**, *83*, 230−244.

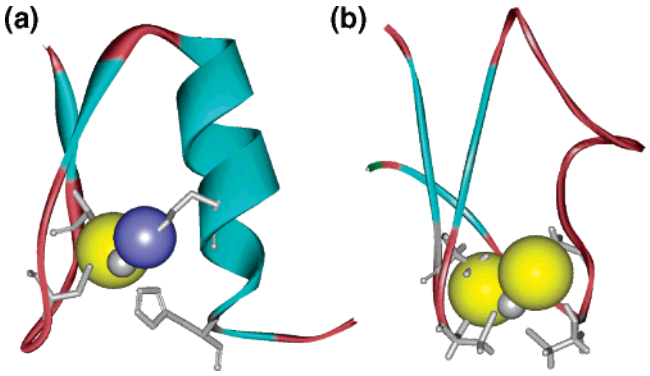

Figure 6. Metal-binding site in the crystal structure of (a) the Zif268 Cys_2-His_2 Zn-finger domain and (b) the Zn−Cys_4 adenylate kinase lid domain, showing the relative sizes of Zn^{2+} (gray), S^- (yellow), and N^- (blue) using vdW radii of 1.57, 3.92, and 3.30 Å, respectively.

sion of the Zn^{2+} CN from four to six in previous Zn protein simulations (see Introduction) is not because the Zn^{2+} vdW parameters have been parametrized to yield a hexahydrated Zn^{2+} in aqueous solution.[35]

Why Does the New PEF with Set A Zn^{2+} vdW Parameters Yield a Tetrahedral Zn−Cys_2His_2 Binding Site, but the Conventional PEF with CHARMM Zn^{2+} vdW Parameters Yields a Nontetrahedral One? The set A Zn^{2+} vdW parameters, which are smaller than the respective CHARMM values, allow closer approach of the Cys^-/His^0 residues to Zn^{2+}, which, in turn, increases their charge transfer to Zn^{2+}. By including charge transfer from S(Cys^-)/N(His^0) to Zn^{2+} in the new PEF, the average Zn charge (1.20e, see **Results**) is significantly less than that (+2e) in simulations using the conventional PEF with the CHARMM force field. Thus, the smaller Zn^{2+} vdW parameters and reduced positive Zn charge in simulations using the new PEF and parameter set A attenuate the net $Zn^{\delta+}$−water interaction energies to such an extent that water molecules are no longer bound to the metal. Although the reduced charges on Zn, S(Cys^-), and N(His^0) likewise attenuate the $Zn^{\delta+}$−Cys^-/His^0 interaction energies, including local polarization of Zn^{2+} and its ligands compensates for this loss, enabling Cys^-/His^0 to remain bound to the metal.

Why does the conventional PEF yield a nontetrahedral Zn−Cys_2His_2 but a tetrahedral Zn−Cys_4 binding site? Clearly, the Zn−Cys_4 binding site differs from the Zn−Cys_2-His_2 one by the substitution of two Zn-bound Cys^- with two His^0 residues. The smaller N (σ_N = 3.30 Å) relative to S^- (σ_S = 3.92 Å) creates space around the Zn cation, allowing water molecules to approach the metal (see Figure 6a). Excluding charge transfer from the ligands to the metal in simulations using the conventional PEF allows the Zn cation to retain the full +2e charge, thus attracting water molecule(s) to the metal. Consequently, in simulations using the conventional PEF (Table 3, MD-$1A_B$, MD-$1B_X$, and MD-$1C_X$) two water molecules become coordinated to Zn^{2+} in addition to the native ligands. On the other hand, in going from a Zn−Cys_2His_2 binding site to a Zn−Cys_4 one, the strong Zn^{2+}-Cys^- charge−charge interactions and steric crowding of the four Cys^- allow simulations with the conventional PEF to retain the observed tetrahedral Zn−Cys_4 geometry (see Figure 6b and Table 4, MD-$1B_X$ and MD-$1C_X$).

Thus, a key factor causing the conventional PEF to yield a nontetrahedral Zn−Cys_2His_2 but a tetrahedral Zn−Cys_4 binding site is the size difference between S(Cys^-) and N(His^0). This is further supported by the finding that simulations including charge transfer and local polarization effects in the PEF with the CHARMM force field do not suffice to reproduce the experimentally observed Zn−Cys_2His_2 geometry (see Table 3, MD-$2B_B$). However, if, in addition to using the new PEF, the vdW radius of N(His^0), σ_N = 3.30 Å, was changed to the value corresponding to that of S(Cys^-), 3.92 Å, while retaining CHARMM values for ϵ_N and for the vdW parameters of Zn^{2+} and S(Cys^-), simulation of the classical zinc-finger domain starting from the end-point of simulation $1B_X$ yielded a tetracoordinated Zn^{2+} structure after ~150 ps.

Biological Significance. Although we have outlined an efficient method for simulating proteins containing Zn−Cys_2-His_2 and Zn−Cys_4 binding sites, the strategy that we have presented in this work is general. It can be used to obtain the force field of Zn^{2+} interacting with protein ligands other than Cys^- and His^0. It can also be used to obtain the force field of other metals interacting with protein ligands that transfer significant amounts of charge to the metal in conjunction with the metal vdW parameters developed in our previous work.[47] Thus, the example shown here for simulations of Zn^{2+} in aqueous solution and "structural" Zn proteins paves the way for accurate simulations of other metalloproteins and metalloenzymes. This is especially important considering that nearly half of all proteins contain metal ions[54] and metal ions perform a wide variety of specific functions associated with life processes.[13,14]

Acknowledgment. We thank Drs. Satheesan Babu and Todor Dudev for helpful discussions. We are grateful to Professor M. Karplus for the CHARMM program. This work is supported by Academia Sinica and the National Science Council, Taiwan.

JA0429115

(54) Thomson, A. J.; Gray, H. B. *Curr. Opin. Struct. Biol.* **1992**, *2*, 155.